Appendix E: Angular studies of Nickel and Nickel-Iron systems

Magneto-transport measurements have been performed while rotating the magnetic field inside the IP plan. This was made in order to get more information about the IP direction. Indeed, the lack of information about this direction yields some difficulties in analysing the sample responses to a magnetic field applied in the IP plan. In this section, one rotates an angle γ that is arbitrarily chosen equal to zero when the magnetic field is perpendicular to the global current flow, which corresponds to the IP direction that was studied in previous subsections.

Figure 80 presents the limit cases A and B presented previously (See Subsection 3.4.1) when rotating the applied magnetic field direction of 90° in the IP plan (i.e. $\gamma = \frac{\pi}{2}$). The applied field direction is then parallel to the global current flow. When one considers the case A, the rotation of the magnetic field direction of 90° yield a different configuration, where, if the magnetisation is saturated in the IP direction, a resistive state $\bar{\rho}_{IP}$, higher than $\rho_\perp$, is reached and defined by:

$$\bar{\rho}_{IP} = \frac{1}{\alpha_m} \int_{\frac{\pi}{2}}^{\frac{\pi}{2}-\alpha_m} \rho_\perp + (\rho_\parallel - \rho_\perp)\cos^2(\alpha) \ \mathrm{d}\alpha \tag{117}$$

which yields

$$\bar{\rho}_{IP} = K_-^{OOP}\rho_\parallel + K_+^{OOP}\rho_\perp \tag{118}$$

With the $K_\pm^{OOP} = \frac{1}{2} \pm \frac{1}{4\alpha_m}\sin(2\alpha_m)$ already defined in Subsection 3.4.1. It means that the resistance state reached when the magnetisation is saturated in this direction $\bar{\rho}_{IP}(\frac{\pi}{2})$ is not equal $\bar{\rho}_{IP}(0)$ previously found in Subsection 3.4.1. As a matter of fact, $\bar{\rho}_{IP}(\frac{\pi}{2})$ and $\bar{\rho}_{IP}(0)$ are expected to be the higher and lower limits of $\bar{\rho}_{IP}(\gamma)$. Therefore, when one rotates the the applied magnetic field direction in the IP plan, a periodic evolution of $\bar{\rho}_{IP}(\gamma)$ with a period of π is expected.

In contrast, when one considers the case B, the rotation of the magnetic field direction of 90° yield a resistive sate at saturation of the magnetisation $\bar{\rho}_{IP}(\frac{\pi}{2})$ identical to $\bar{\rho}_{IP}(0)$. As one can observe in Figure 80, the magnetisations that made an angle β with the NWs axes, now have an angle $\beta+\gamma$, and the magnetisations that made an angle $\beta + \frac{pi}{2}$ with the NWs axis, now have an angle $\beta + \frac{\pi}{2} + \gamma$. In the particular case of $\gamma = \frac{\pi}{2}$, one observes that the two populations of NWs role are inverted. As the NWs are supposed to be randomly and uniformly oriented, the same resistive sate is expected. When rotating the the applied magnetic field direction in the IP plan, one may expect a periodic evolution of $\bar{\rho}_{IP}(\gamma)$ with a period of $\frac{\pi}{2}$.

Analysing the period of the $\bar{\rho}_{IP}(\gamma)$ evolution may show which of the configurations A or B is more adapted for a given sample. Figure 81 presents the evolution of $\frac{\bar{\rho}_{IP}(\gamma)}{\rho_\parallel}$ for Ni (a) and NiFe (b) samples. One can observe a sinusoid evolution in both cases. The period seems to be close to $\gamma = \frac{\pi}{2}$ in the case of Ni. It is less clear in the NiFe sample.

A more general model can be developed to take into account the rotation of $\phi = \beta + \gamma$. It will be derived here for the case B ($\beta = \frac{\pi}{4}$). Figure 82 depicts the general situation. In this situation, the contribution of one NW that has its magnetisation making an angle θ_i with the NWs axisis given by:

$$\rho(\theta_i) = \rho_\perp + (\rho_\parallel - \rho_\perp)\cos^2(\theta_i) \tag{119}$$

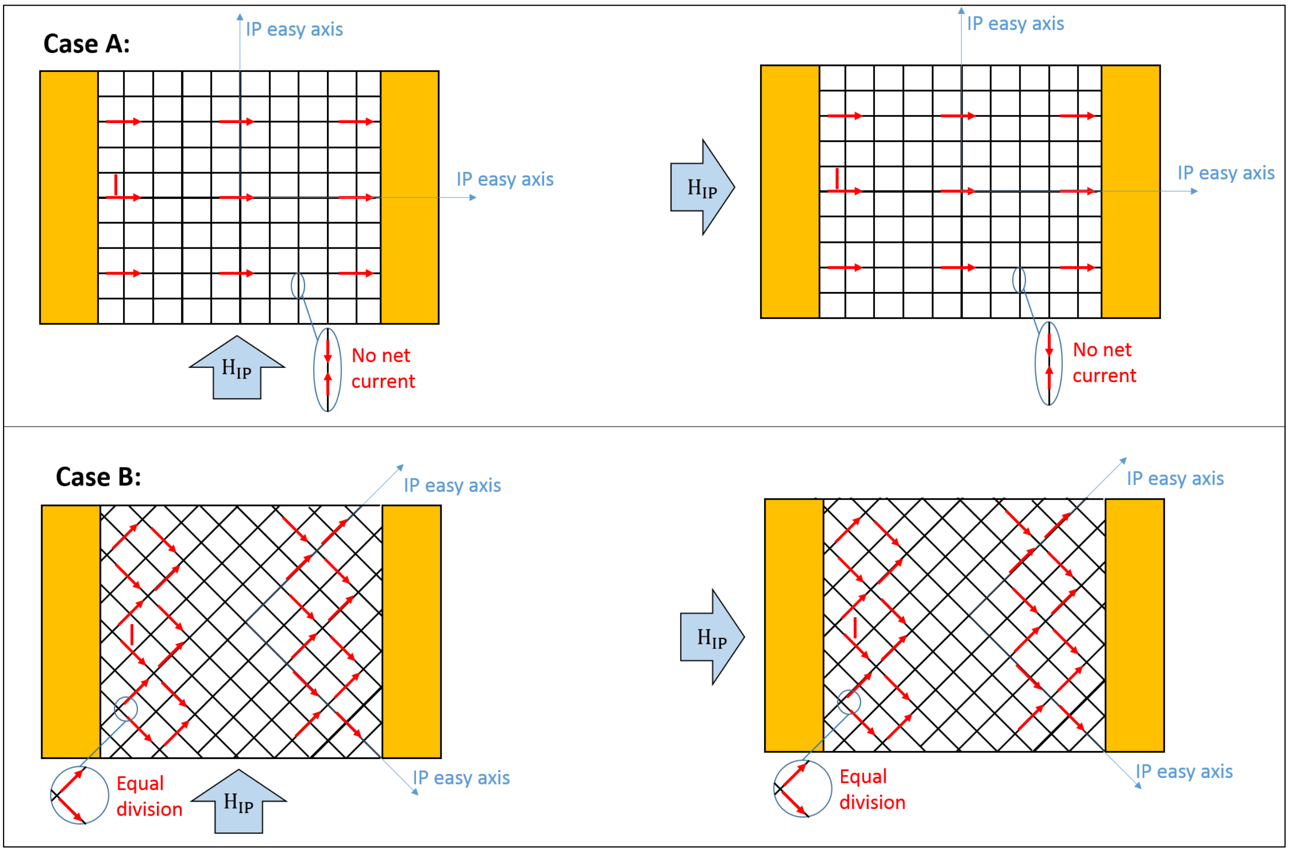

Figure 80: Schematic representation of two IP measuring configurations, one with the applied magnetic field perpendicular to the global current flow, and one with the applied magnetic field parallel to the global current flow for the two limit cases considered. In case A, the 90° rotation of the applied magnetic field in the IP plan yield different resistive state at saturation, while it yields identical resistive sate in case B.

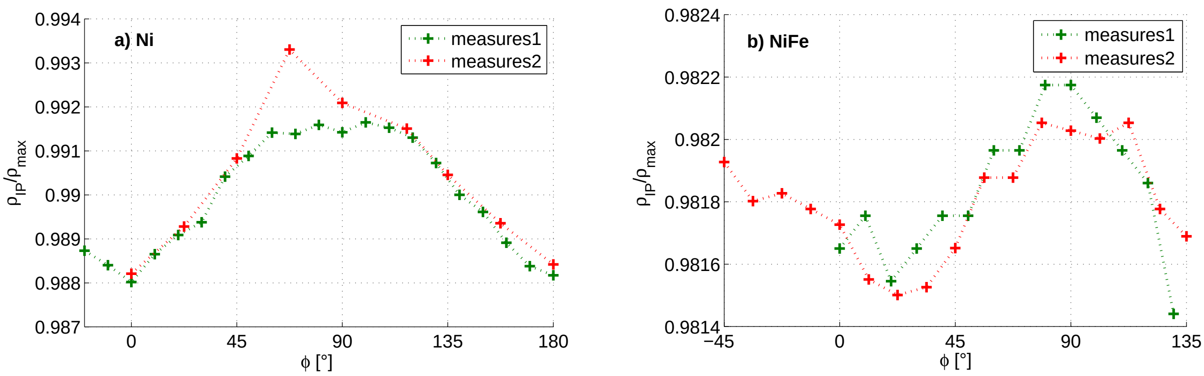

Figure 81: Evolution of $\frac{\bar{\rho}_{IP}(\gamma)}{\rho_{\parallel}}$ for Ni (a) and NiFe (b) samples.

The angle θ_i results from an angle α_i between the NW axis and the OOP direction and an azimuthal angle ϕ_i between the NW and the applied magnetic field. Therefore, one gets:

$$\cos(\theta_i) = \mathbf{j}_{xz} \cdot \frac{\mathbf{M}}{|M|} + \mathbf{j}_{yz} \cdot \frac{\mathbf{M}}{|M|} = \frac{1}{2}(\sin(\alpha_i)\cos(\phi) + \sin(\alpha_i)\sin(\phi)) = \frac{1}{2}(\cos(\phi) + \sin(\phi))\sin(\alpha_i) \tag{120}$$

And thus:

$$\rho(\theta_i) = \rho_\perp + (\rho_\parallel - \rho_\perp)\frac{1}{4}(\cos(\phi) + \sin(\phi))^2 \sin^2(\alpha_i) = \rho_\perp + (\rho_\parallel - \rho_\perp)\frac{1}{4}(\sin(2\phi))\sin^2(\alpha_i) \tag{121}$$

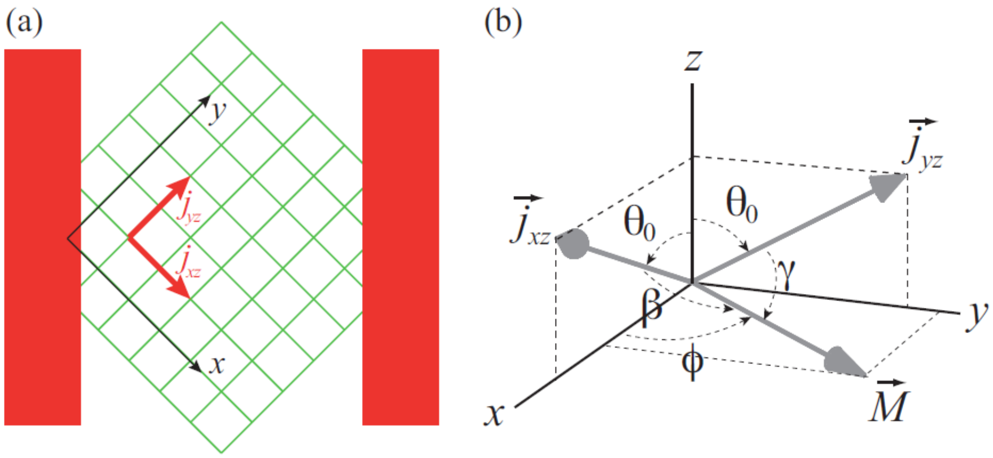

Figure 82: Schematic 3D representation of the general situation presenting a random orientation of the magnetisation $\mathbf{M}$ and the two current $\mathbf{j}_{xz}$ and $\mathbf{j}_{yz}$.

Averaging Equation 121 to take into account the contribution of all the NWs, one gets:

$$\bar{\rho}_{IP}(\phi) = \frac{1}{\alpha_m}\int_0^{\alpha_m} \rho_\perp + (\rho_\parallel - \rho_\perp)\frac{1}{4}(\sin(2\phi))\sin^2(\alpha_i)\ \mathrm{d}\alpha = K_{IP}(\phi)\rho_\parallel + (1 - K_{IP}(\phi))\rho_\perp \quad (122)$$

The constant $K_{IP}(\phi)$, in function of α_m and ϕ, is given by:

$$K_{IP}(\phi) = \frac{1}{4}\left(\frac{1}{2} - \frac{1}{4\alpha_m}\sin(2\alpha_m)\right)(1 + \sin(2\phi)) \quad (123)$$

Finally, one gets:

$$\bar{\rho}_{IP}(\phi) = \rho_\perp + \frac{1}{8}\left(1 - \frac{\sin(2\alpha_m)}{2\alpha_m}\right)(\rho_\parallel - \rho_\perp)(1 + \sin(2\phi)) = C_1 + C_2\sin(2\phi) \quad (124)$$

Therefore, the resistance measured at saturation in function of ϕ is a sinusoidal with a period of $\frac{\pi}{2}$, as expected.

The amplitude of the sinusoidal C_2 can be used to approximate the AMR effect, assuming that $\rho_\parallel$ is known. Indeed, using $\alpha_m = \frac{\pi}{4}$, one has:

$$C_2 = \left(\frac{1}{8} - \frac{1}{4\pi}\right)(\rho_\parallel - \rho_\perp) \quad (125)$$

Which yields:

$$\frac{\rho_\perp}{\rho_\parallel} = 1 - \frac{8\pi C_2}{(\pi - 2)\rho_\parallel} \quad (126)$$

Using the definition of the AMR, one gets:

$$AMR^{IP} = \frac{\frac{8\pi C_2}{(\pi-2)\rho_\parallel}}{\frac{1}{3} + \frac{2}{3}(1 - \frac{8\pi C_2}{(\pi-2)\rho_\parallel})} \quad (127)$$

Table 20 shows the results obtained by applying the model to the measurements of the Ni and NiFe CNWs networks. They are not at all in agreement with what was previously obtained. One may suppose that it is due to the configuration, found to be closer to the case A than the used case B. Note that the value of $\rho_{\parallel}$ may not be perfectly correct=. Indeed, it was only measured before the angular measurements, while the effect of an eventual temperature variation was removed from the angular results, using various measurements of the same $\bar{\rho}_{IP}$ at a given ϕ angle.

Table 20: Calculated $\frac{C_2}{\rho_{\parallel}}$ and AMR^{IP} based on the measurements of $\bar{\rho}_{IP}(\phi)$.

Sample	$C_2/\rho_{\parallel}$	AMR^{IP} [%]
Ni	0.0043 ±0.0011	10.29 ±2.61
NiFe	0.00064 ±0.00013	1.43 ±0.28